Astrophys Space Sci (2019) 364:116
https://doi.org/10.1007/s10509-019-3610-4

ORIGINAL ARTICLE


# Dissipation and reformation of thermal fronts in solar flares

**Jicheng Sun[1,2,3] · Xinliang Gao[1,3] · Quanming Lu[1,3] · Shui Wang[1,3]**

Received: 20 June 2019 / Accepted: 17 July 2019


**Abstract** Thermal fronts are often used to explain the confinement of energetic electrons in the solar corona. In this paper, a 1-D particle-in-cell simulation model is used to explore the evolution of thermal fronts in the flaring magnetic loop. The numerical simulation starts with hot electrons in contact with background cold electrons along the magnetic field. The hot electrons transport along the magnetic field and induce a polarized electric field, drawing a return current from the background cold electrons. This return current can generate ion acoustic waves which could evolve into a double layer (DL). The DL is able to inhibit the transport of electron heat flux, which ultimately leads to the formation of a thermal front. However, the thermal front cannot persist for very long, since the DL will be dissipated by ambient cold protons. As a result, the cold protons trapped within the DL will be efficiently heated. After the vanishing of the first thermal front, hot electrons can again freely expand into the cold plasma, resulting in the growth of ion acoustic waves, which ultimately develop into a new DL. Then, a new thermal front will reform at a location farther into the regions of hot electrons. The new thermal front moves forward $200\lambda_D$ ($\lambda_D$ is the cold electron Debye length) toward the regions containing hot electrons. The implications of simulation results to the observations of hard X-ray emission and confinement of energetic electrons in the corona are also discussed.

✉ X. Gao
gaoxl@mail.ustc.edu.cn

[1] CAS Key Laboratory of Geospace Environment, Department of Geophysics and Planetary Science, University of Science and Technology of China, Hefei 230026, China

[2] Sate Key Laboratory of Space Weather, Chinese Academy of Sciences, Beijing 100190, China

[3] CAS Center for Excellence in Comparative Planetology, Hefei 230026, China

**Keywords** Thermal front · Double layer · Solar flares

## 1 Introduction

During solar flares, coronal electrons can be accelerated to over 100 keV, which is several orders of magnitude higher than the ambient plasma temperature (Lin et al. 2003; Krucker et al. 2007, 2010). Generally, these energetic electrons can emit hard X-ray through interaction with background plasma both in the corona and chromosphere. Observationally it is suggested that the time scale of hard X-ray emissions can be last up to several minutes in the corona (Masuda et al. 1994; Krucker et al. 2007, 2010), indicating that the lifetime of electrons which could produce hard X-ray is two orders of magnitude longer than the free-streaming transit time through the source. Thus, a mechanism must necessarily exist that confines these particles in the source region. The idea of thermal fronts has been brought up to provide a potential mechanism for the confinement of hot electrons in flaring magnetic loops (Brown et al. 1979; Smith and Lillequist 1979). Theoretical analysis shows that expansion of heated electrons into a cool surrounding plasma can generate an acoustic turbulence front which efficiently scatters the electrons, inhibiting the transport of electron heat flux (Brown et al. 1979). Therefore, the decay time of the temperature is increased by a factor $\sim (m_i/m_e)^{1/2}$ over its free-streaming transit time, which is compatible with observations. The observations of hard X-ray emissions also confirm the existence of thermal fronts in solar flares (Rust et al. 1985; Batchelor et al. 1985), suggesting that they may play a dominant role in the transport of energetic electrons from the corona to the chromosphere.

The numerical simulation is a powerful tool to study basic plasma physics in a self-consistent way. But, there

Published online: 26 July 2019

are only several papers relevant to the formation of thermal fronts in flaring magnetic loops using numerical simulation models (Ishigura et al. 1985; McKean et al. 1990; Arber and Melnikov 2009; Li et al. 2012). McKean et al. claimed that a thermal front is not established for a plasma inhomogeneous in electron temperature and homogeneous in density and ion temperature. However, recent simulations (Arber and Melnikov 2009) indicated that the absence of thermal fronts is due to the restricted size of the initial hot-electron region. The thermal fronts can exist actually when larger hot region is used. Moreover, the formation mechanism of thermal fronts has been studied by electromagnetic 2-D (actually 1-D) particle-in-cell simulations (Li et al. 2012). It was shown that the transport of coronal energetic electrons is suppressed by the formation of a DL, which is defined by an electric structure sustaining a potential difference (Block 1978; Raadu and Rasmussen 1988). Karlický (2015) made an extended study of the thermal front formation using a 3-D particle-in-cell simulation. He found that Langmuir and electromagnetic waves can be generated during the formation of thermal fronts.

To better understand the problem of energetic electron transport from the corona to the chromosphere, an important question must be answered that how long the thermal front can exist in the flaring magnetic loops. The previous simulation studies focused mainly on the formation of thermal fronts, while there are little literatures to investigate the dissipation of the thermal front. This paper will fill this gap. Note that our definition of the thermal front refers to the phenomenon that the temperature difference in the plasma is maintained longer than the electron free streaming timescale. We define it in terms of the phenomena rather than from the perspective of physical mechanisms. Here is the organization of the paper. We first describe the simulation model in Sect. 2 and then present simulation results in Sect. 3, followed by conclusions and discussion in Sect. 4.

## 2 Simulation model

A 1-D electromagnetic particle-in-cell simulation model is used to study the self-consistent evolution of thermal fronts, which retains 3-D electromagnetic fields and particle velocities but only 1-D spatial variations in the $x$ direction (Sun et al. 2017). The background magnetic field $\boldsymbol{B_0}$ is oriented in the $x$ direction. The simulation model is performed in a homogenous plasma, and the number density of the plasma is $n_0$. The total length of the computational domain is $L$. For the initial condition, the plasma consists of three components: a Maxwellian distribution of cold electrons and protons, and a bi-Maxwellian distribution of hot electrons. Cold protons and electrons have the same temperature. The hot electrons are distributed in the middle of the computational domain ($L/3 < x < 2L/3$), while the cold electrons are located elsewhere. The parallel temperature of hot electrons is 5 times that of cold electrons, and the perpendicular temperature of hot electrons is equal to that of cold electrons.

In the simulation model, the temperature is normalized to the temperature of cold electrons $T_0$. The time and space are normalized to the inverse of electron plasma frequency $\omega_{pe}^{-1}$ and the Debye length $\lambda_D = v_{t0}/\omega_{pe}$ (where $v_{t0} = \sqrt{T_0/m_e}$ is the thermal speed of cold electrons), respectively. A smaller mass ratio of proton to electron $m_i/m_e = 100$ is chosen just to reduce computational cost. The speed of light $c = 100V_A$ is adopted, where $V_A = B_0/\sqrt{\mu_0 n_0 m_i}$ is the Alfven speed. The cold electron plasma beta is initially set as $\beta_{ec} = 0.4$, and then the Alfven speed is $V_A = 0.224v_{t0}$. The total length of the computational size is $L = 14650\lambda_D$, and the number of grid cells is $n_x = 32768$. Hence, the grid size is set as $\Delta x = 0.447\lambda_D = \lambda_{Dh}$, where $\lambda_{Dh}$ is the Debye length of hot electrons. For each species, there are on average 1000 macroparticles in each cell. The time step is $\Delta t = 10^{-2}\omega_{pe}^{-1}$. The absorbing boundary conditions are used for electromagnetic fields, and reflecting boundary conditions are assumed for particles (Tao 2014).

## 3 Simulation results

With the 1-D particle-in-cell simulation model, we present the evolution of thermal fronts driven by the contact of hot electrons with cold electrons. As a result of the fact that this simulation model is a symmetric system, it is equivalent to analysis either side of the contact. In this paper we choose the right side without any preference, where hot electrons propagate toward the positive direction. For the purpose of illustration, the coordinate of the interface between hot electrons and cold electrons is set to 0. Thus, at the beginning, the coordinates of the location of hot electrons are negative, while the coordinates of the location of cold electrons are positive.

Since the parallel electron transport is of interest, we examine the evolution of electron temperature parallel to the background magnetic field. Figure 1(a) shows the temporal and spatial evolution of electron temperature parallel to the background magnetic field near the region where the interface between hot and cold electrons, and Fig. 1(b) illustrates the spatial profile of electron temperature at $\omega_{pe}t = 0$, 400, 900, and 1500. Note that here the temperature in every grid cell is defined by $T_{e||} = m_e\langle(v_{ex} - \langle v_{ex}\rangle)^2\rangle$, where the angle brackets denote an average over particles inside a cell. Initially, there is a steep temperature gradient between the hot and cold electrons. During a short time ($\omega_{pe}t = 0 \sim 100$), hot electrons expand into the region of cold plasma, which smooths the narrow transition of electron temperature. At $\omega_{pe}t = 400$, a jump emerges in the electron temperature profile near $x = -60\lambda_D$ and remains for a while, which means

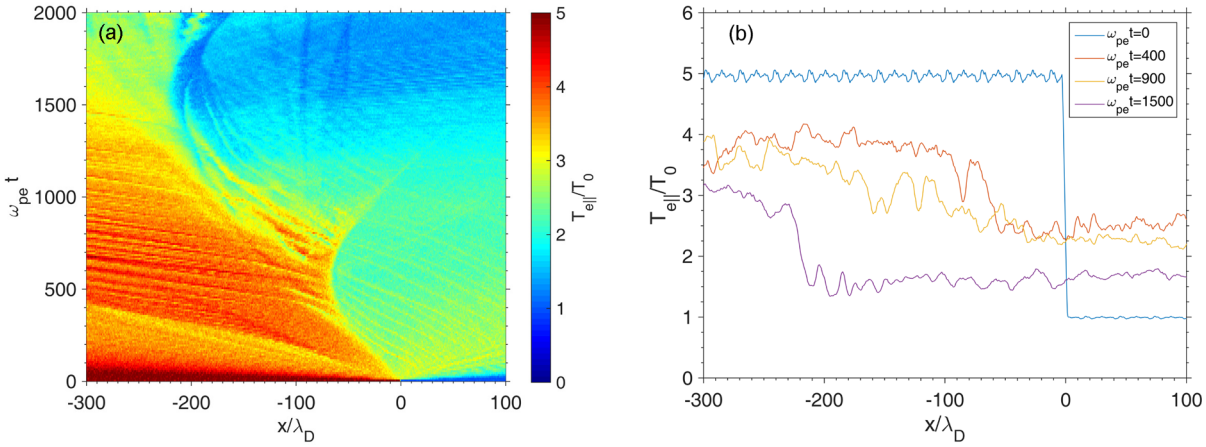


**Fig. 1** (a) The temporal and spatial evolution of electron temperature parallel to the background magnetic field near the transition between hot and cold electrons. (b) The spatial profiles of parallel electron temperature at $\omega_{pe}t = 0$, 400, 900, and 1500

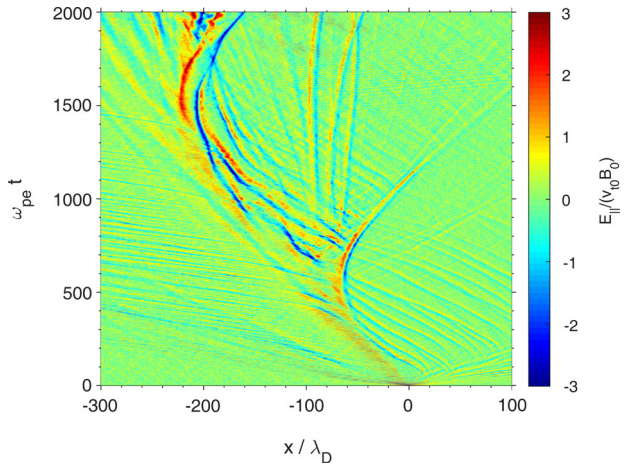


**Fig. 2** The temporal and spatial evolution of the electric field parallel to the background magnetic field

the formation of a thermal front. The appearance of the thermal front indicates that the transport of hot electrons into the cold plasma is suppressed. As time increases, the temperature jump becomes gradual, which suggests that the thermal front is gradually dissipated. At $\omega_{pe}t = 900$, there is no obvious jump in the temperature profile, suggesting that the thermal front has disappeared. It is interesting to note that the thermal front is not absent for a long time. Instead, the thermal front reforms at $\omega_{pe}t = 1500$.

The temporal evolution of the electric field parallel to the background magnetic field is illustrated in Fig. 2. The hot electrons transport along the magnetic field and induce a polarization electric field ($\omega_{pe}t = 0 \sim 200$) because of the charge separation between the expanding electrons and protons. This polarization electric field in turn accelerates ambient cold electrons to form a return current. According to the theoretical analysis by van den Oord (1990), the electromagnetic inductive effect may also play a role in driving the return current. The return current is unstable to excite ion acoustic waves. It is found that the waves are generated at $\omega_{pe}t = 300$, and mainly propagates in the negative direction. By diagnosing the dispersion relation of parallel electric field, the dominant wave mode mainly concentrates at $\omega = 0.6\omega_{pi}$ and $\mathrm{k} = 0.51\lambda_{Dh}^{-1}$, where $\omega_{pi} = 0.1\omega_{pe}$ is the proton plasma frequency. The wave number of the dominant wave mode in our simulation is consistent with that of the fastest growing linear mode ($\mathrm{k} = 0.5\lambda_{Dh}^{-1}$) predicted from theoretical analysis (Manheimer 1977). The phase speed of the dominant wave mode is about $0.26v_{t0}$, which is nearly equal to the ion acoustic speed in the hot electrons region ($v_s = 0.25v_{t0}$). Therefore, it is safe to conclude that the fluctuating electric field in our simulations is indeed ion acoustic waves generated by the return current. The parallel electric field shows significant reduction and enhancement at $\omega_{pe}t = 900$ and 1500, and this is just consistent with the dissipation and reformation of the thermal front.

We have also considered the evolution of the electric potential obtained by integration of the electric field along background magnetic field. Figure 3 displays the spatial profile of electric potential at $\omega_{pe}t = 0$, 400, 900, and 1500. Initially, the electric potentials on both sides of the interface between cold electrons and hot electrons are equal. As the hot electrons transport rightward into the cold plasma, there will be more protons than electrons in the left side. At $\omega_{pe}t = 400$, a DL forms between $x = -100$ and $-50$ $\lambda_D$, which is contributed by the electric field of excited ion acoustic waves. Most of the hot electrons located on the left side cannot pass through the DL, since the potential energy is comparable to the hot electron temperature. Similar to the temperature jump shown in Fig. 1(b), the DL almost completely disappears at $\omega_{pe}t = 900$, which means the DL is dissipated during $\omega_{pe}t = 400$ and 900. The DL then reforms at $\omega_{pe}t = 1500$. The electron temperature jump is consistent with the DL, indicating that the formation of the thermal

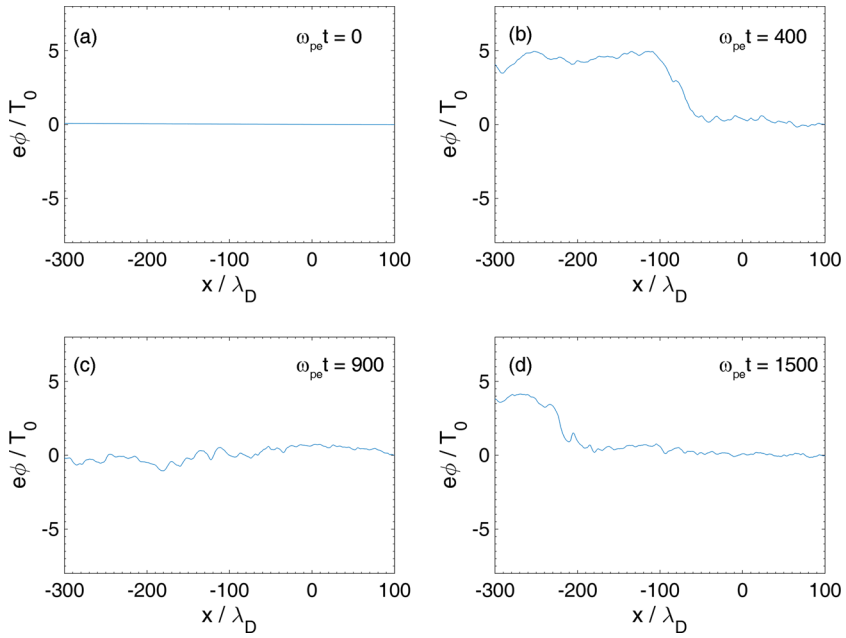


**Fig. 3** The spatial profile of electric potential at $\omega_{pe}t = 0$, 400, 900, and 1500

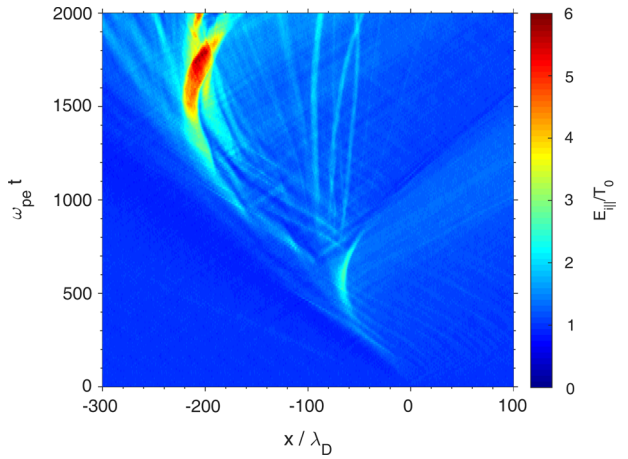


**Fig. 4** The temporal and spatial evolution of parallel kinetic energy for protons

front is caused by the DL. Quantitatively, the suppression of the hot electron transport which has been calculated indicates that the DL can efficiently reduce the electron heat flux by about 50%.

In order to further investigate the dissipation mechanism of the thermal front, we examine the temporal and spatial evolution of parallel kinetic energy for protons in Fig. 4. The parallel kinetic energy in every grid cell is defined by $E_{i||} = m_i \langle v_{ix}^2 \rangle$, where the angle brackets denote an average over particles inside a cell. It can be clearly seen that the protons are heated very effectively. The position and time of proton heating coincide with the position and time of the DL. Moreover, the energy increase of protons ($\sim 3T_0$) is nearly equal to the potential energy decrease of the DL ($\sim 3.5T_0$) shown in Fig. 3. Thus, the DL is dissipated by the cold protons, which can lead to the dissipation of the thermal front. It is worth noting that, in our simulation, the proton energization by the second DL is more efficient than it is by the first DL, because of the greater electric field of the second DL.

To study the reformation mechanism of the thermal front, we also investigate the particle dynamics in the simulation. Figure 5 shows the phase space of protons (left column) and electrons (right column) at $\omega_{pe}t = 400$, 900, and 1500. At $\omega_{pe}t = 400$, the protons with positive velocities between $x = -100$ and $-50\lambda_D$ are effectively accelerated by the DL, while the protons with negative velocities are significantly slowed down by the DL. The cold electrons on the right side move toward the left side and form a return current at $x > -50\lambda_D$, and the narrow electron beam at $x < -50\lambda_D$ is attributed to the acceleration by DL. The growth of streaming instability excited by the return current depends on the return current intensity. We can see that the return current is strong at this time, leading to a large amplitude electric field of ion acoustic waves. At $\omega_{pe}t = 900$, the return current intensity has been significantly reduced, resulting in the saturation of streaming instability. The DL leads to the effective heating of the cold protons. In turn, the DL is dissipated, which causes the disappearance of the thermal front. The thermal front has disappeared, but it can be seen from Fig. 1(b) that the temperature gradient of electrons still exist. At this time, electrons in the left side can move up to right freely without any restriction by electric field, similar to the initial time, which can promote the enhancement of return current. This return current can excite the ion acoustic waves again, which can evolve into a new DL. At $\omega_{pe}t = 1500$, there is a significant jump in the electron temperatures between $x = -220$ and $-200\lambda_D$, suggesting the reformation

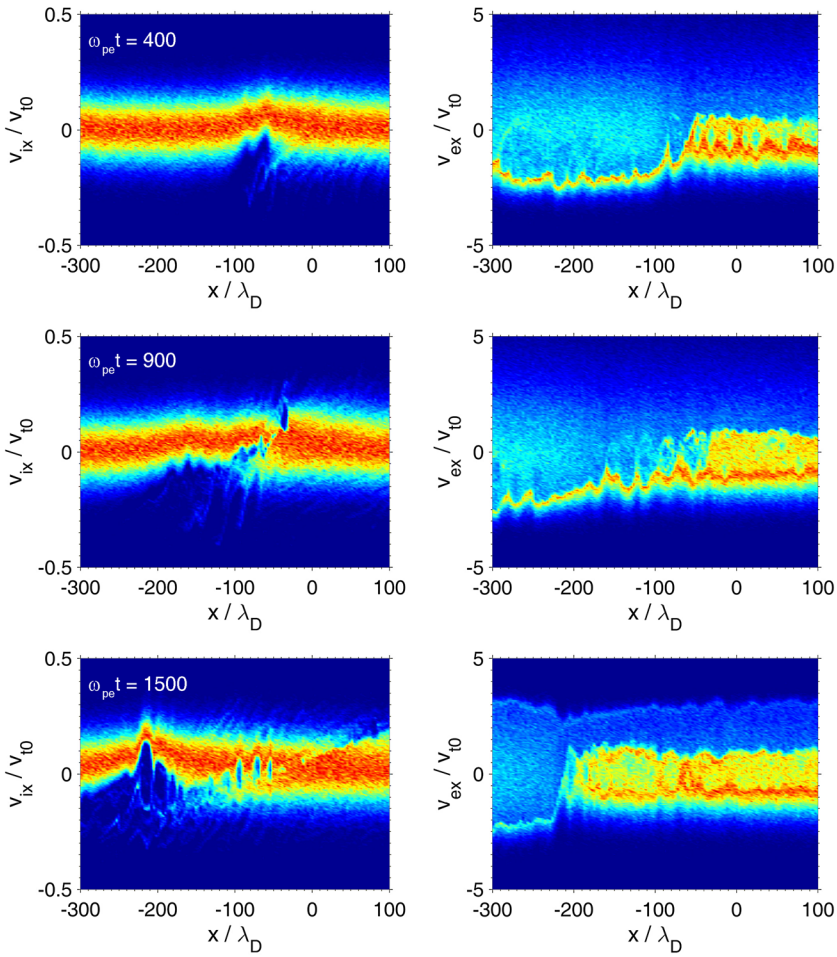


**Fig. 5** The phase space of protons (left column) and electrons (right column) at $\omega_{pe}t = 400$, 900, and 1500

of the thermal front. Moreover, the protons are accelerated again around $x = -220\lambda_D$.

Although the mass ratio used in our simulation is reduced, the dissipation and reformation of the thermal front still exist in the case of real mass ratio. Figure 6(a) illustrates the time evolution of the parallel electric field for the case of the real mass ratio. Figure 6(b) and 6(c) show the corresponding time evolution of the parallel temperature for electrons and the parallel kinetic energy for protons, respectively. Similar to the result of a mass ratio of 100, the evolution of DL also shows the dissipation and reformation processes, and the time periods of these two processes now become longer. The lifetime of the first DL can last up to about $\omega_{pe}t = 4000$, which is about 4 times that in the case of the smaller mass ratio. This indicates that the existence time of a thermal front is proportional to $\sqrt{m_i}$. At $\omega_{pe}t = 5000$, the DL forms again. The time of reforming the DL becomes longer, which results in a smaller temperature gradient of the electron in the second formation (Fig. 6b). Thus, the second formation of DL appears weaker than the first formation. Compared with the first formation, the second DL moves about $200\lambda_D$ toward the left region, which is similar to the case of the reduced mass ratio. This is because the speed of ion acoustic waves is inversely proportional to $\sqrt{m_i}$. It can be seen from Fig. 6(b) that the characteristic time of a single thermal front confining electron can reach 4000 $\omega_{pe}^{-1}$. Therefore, the thermal front is more efficient at inhibiting the transport of hot electrons in the real mass ratio case. The time and location of protons heating in Fig. 6(c) are consistent with those of DL. In addition, the second proton heating is weaker than the first proton heating since the second DL is weaker than the first one.

## 4 Conclusions and discussion

With a 1-D particle-in-cell simulation model, we have investigated the evolution of thermal fronts in the system of hot electrons in contact with ambient cold electrons along the magnetic field. The hot electrons transport along the magnetic field and induce a polarization electric field, drawing a cold electron return current from the background cold plasma. This return current is able to excite ion acoustic waves, which could develop into a DL. The DL can inhibit the transport of electron heat flux, which can contribute to the formation of a thermal front. Later the DL leads to the

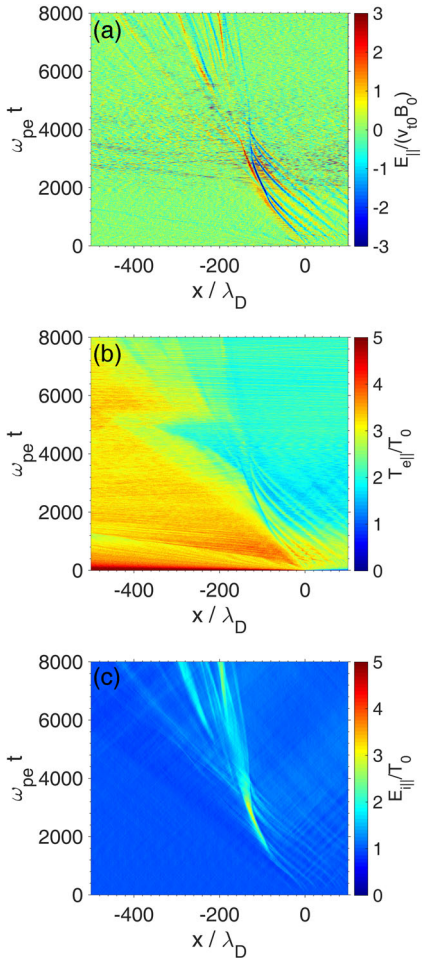


**Fig. 6** The temporal and spatial evolution of (a) the parallel electric field, (b) the parallel temperature of electrons, and (c) the parallel kinetic energy of protons for the case of the real mass ratio

effective energization of the cold protons, thus dissipating this DL. This will cause the disappearance of the thermal front. After the first thermal front vanishes, hot electrons can again freely expand into the cold plasma, leading to the growth of ion acoustic waves. These waves finally develop into a new DL. Then, a new thermal front will reform at a location farther into the regions of hot electrons. The reformation mechanism is similar to the formation mechanism. The new thermal front moves about $200\lambda_D$ to the side of the hot electrons. In addition, we have considered the effects of proton to electron mass ratio on the thermal front by another simulation, where the mass ratio is realistic. With the increase of mass ratio, the existence time of a thermal front becomes longer, which could cause this thermal front to contain the transport of hot electrons more efficiently.

In this paper, the result that the formation of thermal fronts is caused by the DL is consistent with that of Li et al. (2012). In addition, we have further investigated the evolution of thermal fronts. We find that the thermal front cannot exist for very long as the DL will be dissipated by ambient cold protons. After the first thermal front vanishes, ion acoustic waves grow when hot electrons can again freely expand into the cold plasma, resulting in the formation of a new DL. Then, a new thermal front will reform at a location farther into the regions of hot electrons. Therefore, the thermal front will experience the cyclic reformation process during the expansion of hot electrons. The results obtained in this paper provide valuable insights to understand the electron dynamics during solar flares, including the dissipation and reformation of thermal fronts.

A thermal front forms between hot and cold electrons, and it may play an important role to confine energetic electrons in solar fares. These energetic electrons are produced by magnetic reconnection (Fu et al. 2006; Wang et al. 2010a; Lu et al. 2010; Wang et al. 2010b). The DL has also been in situ observed in the separatrix region during magnetic reconnection (Wang et al. 2014), while our simulation shows that such kind of DLs may be caused by the electron temperature gradient. As typical parameters of coronal X-ray sources, the cold electron temperature is 1 keV and the plasma number density is $10^9$ cm$^{-3}$. So, the cold electron Debye length should be 0.01 m, and the computational size of the particle-in-cell simulations is about 150 m. It is very small compared to the realistic size of flaring loops which is about tens of thousands of kilometers. However, we believe that the simulation may show the physical processes near the interface between hot and cold electrons. Since each thermal front exists for only about 1000 electron-plasma periods ($\sim 10^{-5}$ s), we suggest that the confinement of hot electrons in the corona can be caused by a series of thermal fronts. The formation mechanism of each thermal front is the same, and hence the lifetime of each thermal front should be quite similar. In the simulation, the reformed thermal front moves about $200\lambda_D$ toward to the region of hot electrons. Considering realistic solar flares, this means the region of hot electrons will shrink about 2 meters in $10^{-5}$ s. Thus, for a flaring magnetic loop of $10^7$ m, the total thermal electron transport time scale can reach up to tens of seconds, which can explain the prolonged decay time of X-ray emissions in the solar corona. It is interesting to note that magnetic mirror may also plays a significant role in confinement of electrons in the corona. Self-consistent simulations of the combined effects of thermal fronts and magnetic mirror will be performed in future works.

**Acknowledgements** This work was supported by the NSFC grant 41527804,41774151, 41604128, 41631071, 41474125, Specialized Research Fund for State Key Laboratories, Youth Innovation Promotion Association of Chinese Academy of Sciences (No. 2016395), Young Elite Scientists Sponsorship Program by CAST (2018QNRC001), and Key Research Program of Frontier Sciences, CAS (QYZDJ-SSW-DQC010).

## References


Arber, T.D., Melnikov, V.F.: Astrophys. J. **690**, 238 (2009)
Batchelor, D.A., Crannell, C.J., Wiehl, H.J., Magun, A.: Astrophys. J. **295**, 258 (1985)
Block, L.P.: Astrophys. Space Sci. **55**, 59 (1978)
Brown, J.C., Melrose, D., Spicer, D.S.: Astrophys. J. **228**, 592 (1979)
Fu, X.R., Lu, Q.M., Wang, S.: Phys. Plasmas **13**, 012309 (2006)
Ishigura, S., Kamimura, T., Sato, T.: Phys. Fluids **28**, 2100 (1985)
Karlický, M.: Astrophys. J. **814**, 153 (2015)
Krucker, S., et al.: Astrophys. J. **714**, 1108 (2010)
Krucker, S., White, S.M., Lin, R.P.: Astrophys. J. Lett. **669**, L49 (2007)
Li, T.C., Drake, J.F., Swisdak, M.: Astrophys. J. **757**, 20 (2012)
Lin, R.P., et al.: Astrophys. J. Lett. **595**, L69 (2003)
Lu, Q.M., et al.: J. Geophys. Res. **115**, A11208 (2010)
Manheimer, W.M.: Phys. Fluids **20**, 265 (1977)
Masuda, S., Kosugi, T., Hara, H., Tsuneta, S., Ogawara, Y.: Nature **371**, 495 (1994)
McKean, M.E., Winglee, R.M., Dulk, G.A.: Astrophys. J. **364**, 295 (1990)
Raadu, M.A., Rasmussen, J.J.: Astrophys. Space Sci. **144**, 43 (1988)
Rust, D.M., Simnett, G.M., Smith, D.F.: Astrophys. J. **288**, 401 (1985)
Smith, D.F., Lillequist, C.G.: Astrophys. J. **232**, 582 (1979)
Sun, J.C., et al.: J. Geophys. Res. Space Phys. **122**, 5377–5390 (2017)
Tao, X.: J. Geophys. Res. Space Phys. **119**, 3362–3372 (2014)
van den Oord, G.H.: A&A **234**, 496 (1990)
Wang, R.S., et al.: Geophys. Res. Lett. **41**, 4851–4858 (2014)
Wang, R.S., Lu, Q.M., Huang, C., Wang, S.: J. Geophys. Res. **115**, A01209 (2010a)
Wang, R.S., Lu, Q.M., Du, A.M., Wang, S.: Phys. Rev. Lett. **104**, 175003 (2010b)